Petrology, Vol. 12, No. 3, 2004, pp. 227–243. Translated from Petrologiya, Vol. 12, No. 3, 2004, pp. 264–280.

Structural and Compositional Characteristics of the Oldest Volcanic Glass in the Early Paleoproterozoic Boninite-Like Lavas of Southern Karelia

E. V. Sharkov, N. V. Trubkin, I. S. Krassivskaya, O. A. Bogatikov, A. V. Mokhov, A. V. Chistyakov, and K. A. Evseeva

Institute of Geology of Ore Deposits, Petrography, Mineralogy, and Geochemistry (IGEM), Russian Academy of Sciences, Staromonetnyi per. 35, Moscow, 119017 Russia
e-mail: sharkov@igem.ru

Received April 10, 2003

Abstract—The oldest volcanic glass in the uniquely fresh siliceous high-Mg (boninite-like) lavas of the Vetrenyi Poyas complex with an age of about 2.41 Ga from the Vetrenyi Poyas rift structure in Karelia was studied for the first time by instrumental methods using a JEM-100C transmission electron microscope with a Kevex-5100 energy-dispersive X-ray spectrometer. Two types of glass were distinguished: (1) basic glass representing portions of initial magmatic melt that had not enough time to crystallize and (2) residual glass occurring in interstices between microspinifex-textured pyroxene and olivine crystals; the latter glass varies in composition from andesite to dacite. It was found that the volcanic glass is composed of amorphous silica containing nanocrystals of hydrous silicates (amphiboles and various phyllosilicates), orthopyroxene, α-quartz, and tridymite and rare grains of halite, anatase, and cuprite. The mineralogical composition of these nanophases is sharply different from the association of phenocrysts and groundmass crystals of the lava, which comprises olivine, aluminous clinopyroxene, plagioclase, and chromite. The nonuniform distribution of nanophases in the glass provides its mottled appearance in back-scattered electron images and variable compositions determined by the electron microprobe. Their distribution is not related to secondary processes but reflects the primary heterogeneity of the melt preserved owing to rapid quenching. The nature of these nanophases is not yet clear. They could be the products of crystallization of partially ordered silicate micelles in a siliceous matrix, which occurred both immediately after glass quenching in a hot material (orthopyroxene, tridymite, and α-quartz) and during subsequent cooling and prolonged evolution in the Earth's crust under much lower temperature conditions, when other nanocrystals were formed.

INTRODUCTION

Early Precambrian volcanic rocks are usually strongly altered by secondary processes, and their initial compositions and structural features are only very rarely preserved. Among such rare cases are Early Paleoproterozoic basalts with volcanic glass from the Vetrenyi Poyas complex occurring in the rift structure of the same name in southeastern Karelia. These rocks were first described by Kulikov (1988), and their geochemistry and isotopic systematics were characterized by Puchtel *et al.* (1997, 2001). The latter authors also determined the isotopic ages (Sm–Nd, Re–Os, and U–Pb zircon systems) of volcanic rocks from this complex as 2.45 Ga for the lower part of the section and 2.41 Ga for the upper part.

These volcanics were also studied by Zolotykh and Ladygin (2000, 2001), who determined their compositions and physical properties with application to practical use. Their results also confirmed the presence of volcanic glass in the rocks. This complex was additionally sampled by us during the short-term fieldwork of 2000 in the extreme southeastern part of the Vetrenyi Poyas structure, where the freshest rocks were found. The samples were studied mostly at the Institute of Geology of Ore Deposits, Petrography, Mineralogy, and Geochemistry, Russian Academy of Sciences.

Prior to our study, volcanic glass was identified in these rocks by petrographic methods only, and there was a need for more reliable characterization of this material by modern physical techniques and determination of its structural characteristics.

OVERVIEW OF THE GEOLOGIC SETTING AND ROCKS OF THE VETRENYI POYAS COMPLEX

During the Early Paleoproterozoic (2.5–2.3 Ga), a large magmatic province of siliceous high-magnesia (boninite-like) series was formed in the eastern part of the Baltic shield (Sharkov *et al.*, 1997). It was made up of layered mafic–ultramafic intrusions, dike swarms, and volcanosedimentary complexes in grabenlike structures, which are exemplified by the Vetrenyi Poyas complex (Fig. 1). This province is similar in geologic setting and size to the Phanerozoic large igneous provinces related to the activity of superplumes, such as the

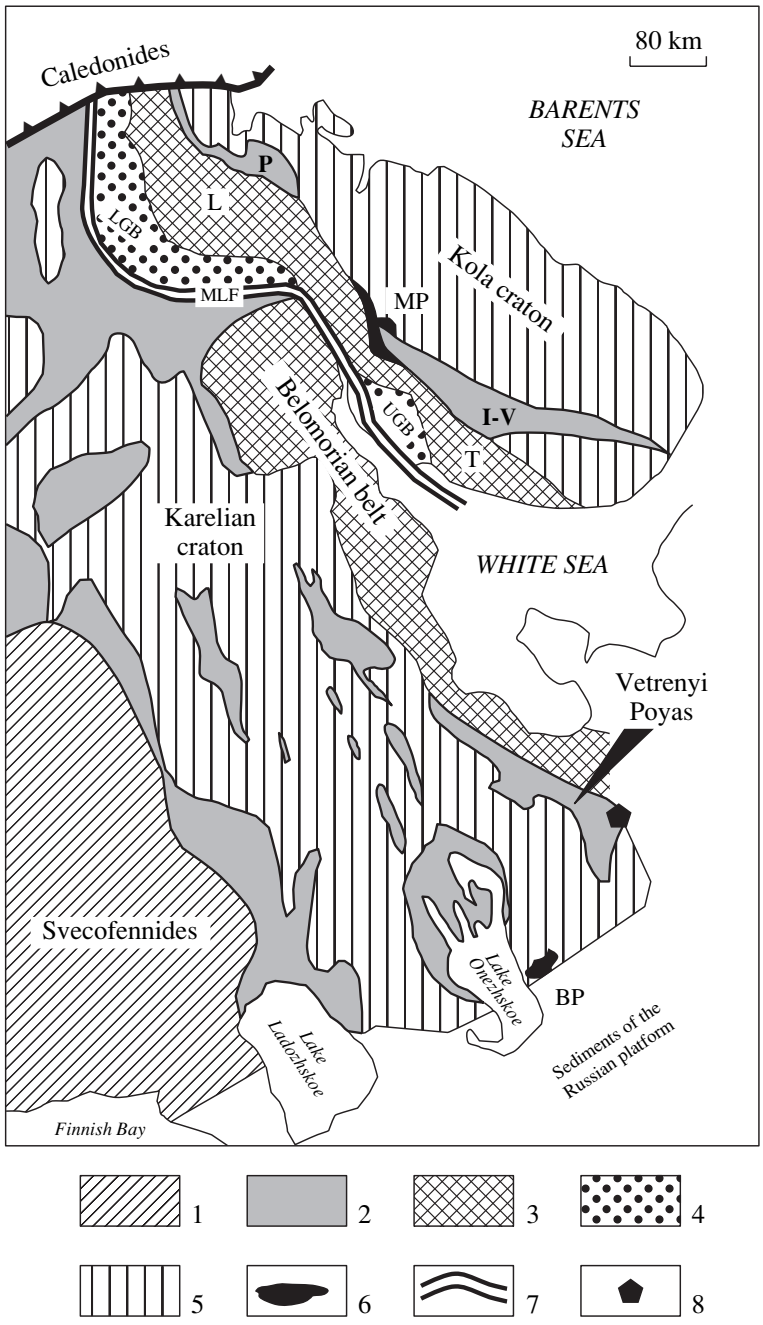

Fig. 1. Schematic geologic structure of the eastern Baltic shield. (1) Svecofennian block; (2) Paleoproterozoic volcanosedimentary belts (P, Pechenga and I–V, Imandra–Varzuga); (3) mobile belts: Belomorian and Tersko (T)–Lottinskii (L); (4) Lapland–Umbina granulite belt (LGB, Lapland and UGB, Umbina segments); (5) Archean cratons; (6) Early Proterozoic layered intrusions (MP, Monchegorsk and BP, Burakovskii plutons); (7) Main Lapland Fault (MLF); and (8) Myandukha Mountain.

Siberian trap province, but the compositions of rocks are very different.

The Vetrenyi Poyas volcanics resemble the high-calcium boninites of the Izu–Bonin arc (Murton *et al.*, 1992) with respect to composition (high *mg*-numbers of mafic minerals, presence of andesitic glass, and geochemical characteristics) and peculiar feather microtextures. Such a resemblance does not however imply their consanguinity, because the Precambrian rocks studied were formed in an intraplate continental environment in contrast to the similar Phanerozoic complexes. Their generation was connected with the extensive assimilation of lower crustal material by ascending hot mantle-derived melts through the zone melting mechanism (Sharkov *et al.*, 1997). Such a tec-

tonomagmatic activity was characteristic of the Early Paleoproterozoic in all Precambrian shields, and the Baltic shield is not an exception (Bogatikov *et al.*, 2000).

At the age boundary 2.0–1.9 Ga, the shield was affected by extensive tectonic processes related to the opening of the Svecofennian ocean in its central part and formation of the Lapland–Kola collision zone in its eastern margin, in the Kola Peninsula northeast of the Main Lapland Fault (Sharkov *et al.*, 2000). These processes were accompanied by the appearance of numerous tectonic dislocations, which produced dynamometamorphic transformations in some rocks of the province adjacent to the collision zone. Structures occurring in tectonic shadows were least affected by these processes. Among them is the Vetrenyi Poyas, whose rocks are almost unaltered in places.

PETROGRAPHIC DESCRIPTION

We studied rocks from the upper part of the Vetrenyi Poyas section at the southeastern end of the grabenlike structure of the same name, in the region of Myandukha Mountain. A volcanic sequence consisting of seven gently sloping basaltic flows with a total thickness of about 200 m was distinguished there. The presence of pillow lavas and hyaloclastites suggests that the lavas erupted in a submarine environment. The rocks are locally overprinted by superimposed low-temperature processes, which produced fibrous actinolite, chlorite, serpentine, talc, etc. Very fresh varieties were found in places with well preserved primary magmatic minerals and volcanic glass. There are a number of varieties differing in mineral composition and abundance of volcanic glass.

The rocks often show porphyritic textures with phenocrysts of olivine and, occasionally, pyroxene and microphenocrysts of chromite (Fig. 2). The most remarkable feature of the rock groundmass is the occurrence of microspinifex textures, which are characterized by the development of needlelike prismatic crystals and fibrous, radial, and feather aggregates of clinopyroxene (augite and pigeonite) and, occasionally, plagioclase, and skeletal pyroxene grains in volcanic glass. Calcic plagioclase was identified in the most crystallized varieties. The minerals were analyzed on an MS-46 Cameca electron microprobe at the Institute of Geology of Ore Deposits, Petrography, Mineralogy, and Geochemistry, Russian Academy of Sciences (Tables 1–4).

Fresh olivine from the porphyritic grains varies in composition from Fo_{83} to Fo_{63}. The composition of clinopyroxene corresponds to aluminous augite, $Wo_{45–47}En_{33–42}Fs_{12–21}$ with 6.5–10.5 wt % Al_2O_3; pigeonite, $Wo_{11}En_{60}Fs_{29}$ with 4.3 wt % Al_2O_3; and pigeonite–augite (subcalcic augite), $Wo_{30–42}En_{44-53}Fs_{10-19}$ with 1.5–6.0 wt % Al_2O_3. The component compositions of the pyroxenes are shown in Fig. 3. Chrome spinel con-

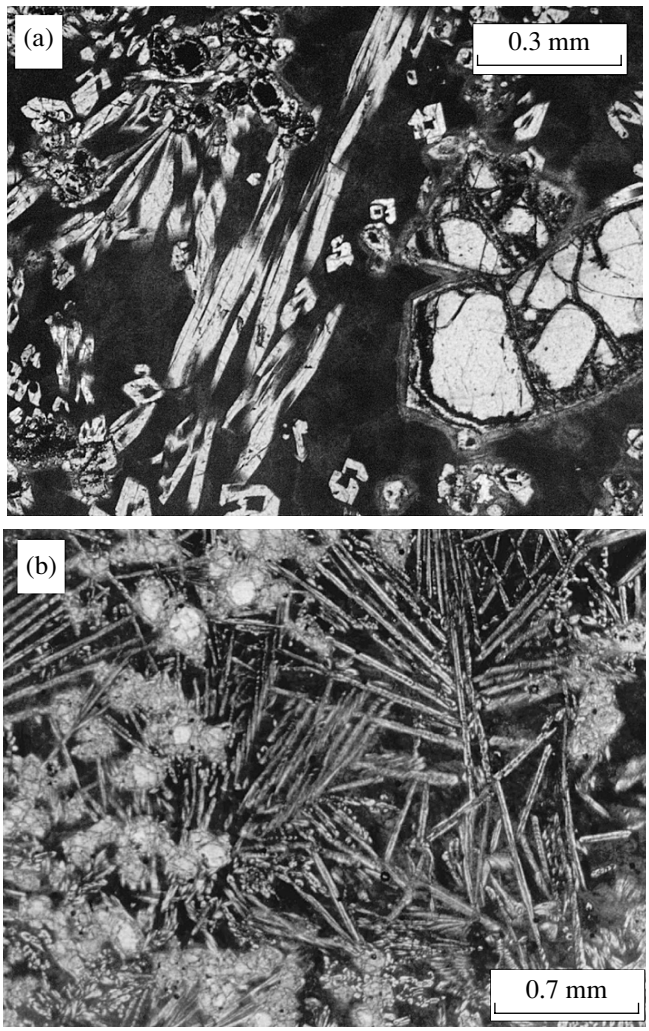

Fig. 2. Photomicrographs of thin sections of basalts (plane-polarized light). (a) Olivine phenocrysts and randomly oriented skeletal clinopyroxene grains in glass (dark), sample 71. (b) Clinopyroxene microspinifex texture in volcanic glass (dark background); small light grains are olivine, sample 323.

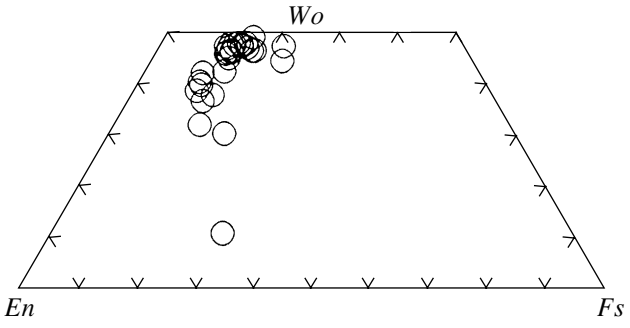

Fig. 3. Compositions of clinopyroxenes from the basalts on the *En–Wo–Fs* diagram.

Table 1. Compositions (wt %) of olivine phenocrysts from the olivine–clinopyroxene basalts of Myandukha Mountain

Component	Sample no.												
	323-1	323-2	323-3	323-4	100-1	100-1a	100-2	100-3	100-4	100-5	100-6	100-7	33
SiO_2	37.65	36.13	38.08	35.79	38.94	38.29	37.37	36.75	38.90	36.70	35.92	36.96	35.87
FeO_{tot}	18.55	22.41	19.97	21.37	15.77	17.11	19.45	26.09	18.40	28.23	30.96	26.45	32.44
MnO	0.25	0.32	0.27	0.32	0.22	0.27	0.31	0.43	0.28	0.27	0.45	0.43	0.49
MgO	41.54	39.35	41.47	41.76	44.03	43.41	42.85	35.52	41.88	33.88	32.02	35.04	30.66
CaO	0.27	0.27	0.25	0.25	0.29	0.27	0.22	0.24	0.22	0.16	0.50	0.22	0.12
NiO	0.20	0.14	0.15	0.15	0.18	0.17	0.19	0.14	0.15	0.14	0.16	0.16	0.00
Total	98.46	98.62	100.19	99.64	99.43	99.52	100.39	99.17	99.82	99.36	100.01	99.25	99.57
Fo	0.80	0.76	0.79	0.78	0.83	0.82	0.80	0.71	0.80	0.68	0.65	0.70	0.63

tains from 43.5 to 45.1 wt % Cr_2O_3, and plagioclase is labradorite, $Or_1Ab_{35–37}An_{62–64}$. Minerals with similar compositions are common in high-calcium boninite lavas, for instance, in the Izu–Bonin arc (Murton *et al.*, 1992) and the Late Cretaceous ophiolitic association Bassit in Syria (Sharkov and Sindeev, 1987).

It is noteworthy that strongly crystallized basalts, e.g., samples 39 and 99 (Table 2), contain pyroxenes with very low Al_2O_3 contents, close or not much higher than the ordinary values of igneous pyroxenes. The highest Al_2O_3 contents were detected in the pyroxenes forming microspinifex textures in glassy groundmass (samples 323, 33, 71, and 100; Table 2). Such aluminous compositions of pyroxenes were probably related to their crystallization under conditions of strong supercooling. Their compositions are similar to those of experimental quench pyroxenes reported by Babansky *et al.* (1983), although they are lower in Ca content.

Volcanic glass occurs in hyalocrystalline lavas and hyaloclastites. It is brown in plane-polarized transmitted light and isotropic or slightly anisotropic in cross-polarized light. In the latter case, the glass exhibits mosaic or spotted fragmentation, sometimes with weak undulating extinction reminiscent of perlitic fabrics. The volcanic glass of the hyaloclastites shows a very fine fluidal banded structure, which is visible even at the micrometer level (Fig. 4).

Two types of volcanic glass were found: (1) irregular patches between crystallized portions of lavas with embayed boundaries (Fig. 5) and (2) glass in the groundmass in the interstices between microspinifex pyroxene crystals and olivine phenocrysts (Fig. 2).

GEOCHEMICAL CHARACTERISTICS OF THE ROCKS

The chemistry of the rocks is characterized by ten analyses obtained by traditional chemical methods and 30 XRF determinations on a PW 2400 Philips spectrometer recalculated to totals of 100%. Tables 5–7 show that all the basalts have low TiO_2 contents (0.6–0.7 wt %), high SiO_2 (more than 50 wt %), and MgO between 8 and 19 wt %. In the binary diagrams (Fig. 6) of the major components CaO, Al_2O_3, TiO_2, SiO_2, FeO_{tot}, and Na_2O versus MgO, the rocks form almost linear gently sloping trends. The Myandukha basalts have gently sloping REE distribution spectra with a significant enrichment in light REE, $(La/Nd)_n$ = 1.72–1.76 (Table 8, Fig. 7). All these characteristics are indicative of boninite-like magmatic melts, which are common in all complexes of the siliceous high-magnesia series (SHMS) of the Early Paleoproterozoic Baltic province (Sharkov *et al.*, 1997). The concentrations of trace elements in the rocks studied are also similar to those of the Izu–Bonin boninites (Fig. 8).

These diagrams (Fig. 6) also show the microprobe analyses of volcanic glasses from the basalt groundmass and hyaloclastites (Table 9). The above-mentioned two types of glasses are also different in chemical composition. Glasses of the first group occur as irregular patches between crystallized areas in the hyaloclastites and basalts (Fig. 4). They are rare and have basic compositions similar to those of the rocks. Their SiO_2 content varies from 46 to 54 wt % (Table 9, an. 303, 33; Fig. 6). High-magnification images of these glasses display fine spotty textures, with light and dark areas of different compositions (Fig. 5; Table 9, an. 303). These glasses were evidently formed through very rapid quenching of a basaltic melt, which was practically not affected by crystallization.

Glasses of the second group are more abundant in the lavas (30–40 vol %). They show more silicic compositions approaching andesite and dacite, and their SiO_2 content varies from 56–57 to 62 wt % (Table 9). These glasses are enriched in Al_2O_3 (17–21 wt %) and Na_2O (up to 9 wt %) and depleted in MgO (0.5–6.0 wt %). Their points form separate cluster in the diagrams (Fig. 6) far from the compositions of the host basalts. In contrast to the rocks, the glasses show rough positive correlations CaO–MgO and FeO–MgO. Taking into

Table 2. Compositions of pyroxenes (wt %) from the basalts of Myandukha Mountain

Component	Sample no.														
	323-1	323-2	323-3	323-4	323-5	1	33-1	33-2	33-6	39-1	39-2	39-3	71-1	71-2	71-3
SiO_2	50.83	49.85	49.15	49.59	48.97	54.12	46.95	48.33	47.12	52.69	51.79	51.81	48.82	49.01	49.16
TiO_2	0.90	0.85	0.75	0.85	1.03	0.06	0.94	0.91	0.97	0.37	0.35	0.33	0.72	0.65	0.83
Al_2O_3	6.65	6.88	7.52	7.90	7.22	4.35	9.38	9.76	10.65	2.02	3.29	3.23	6.42	5.84	6.95
FeO_{tot}	7.62	8.98	7.62	8.53	11.46	15.92	8.81	9.13	11.64	8.59	6.34	6.24	7.14	7.17	7.71
Cr_2O_3	0.32	–	–	0.18	0.28	0.16	0.28	–	–	0.19	0.79	0.83	0.19	0.16	0.22
MnO	0.21	0.21	0.21	0.19	0.28	0.52	–	–	–	0.22	0.18	0.17	0.15	0.19	0.21
NiO	–	–	–	–	–	0.14	–	–	–	–	–	–	–	–	–
MgO	13.63	12.5	13.8	12.37	9.55	18.88	11.34	11.1	9.56	17.13	17.25	16.83	13.76	13.95	14.34
CaO	21.38	21.65	21.79	21.94	20.15	4.78	21.63	19.57	17.75	18.69	19.67	17.84	21.31	22.19	21.31
Na_2O	0.27	0.23	0.31	0.24	0.30	0.86	–	0.60	1.34	0.07	0.13	0.05	0.12	0.09	0.20
Total	101.81	101.15	101.15	101.79	99.24	99.79	99.33	99.41	99.03	99.97	99.79	97.33	98.63	99.25	100.93
Wo	46.0	46.9	45.5	47.7	47.3	10.9	48.8	46.5	44.2	37.8	40.3	38.6	46.2	46.9	44.9
En	40.8	37.6	40.1	37.4	31.2	59.9	35.6	36.6	33.1	48.2	49.2	50.6	41.5	41.0	42.1
Fs	13.2	15.5	14.4	14.8	21.5	29.3	15.5	16.9	22.6	13.9	10.4	10.8	12.3	12.1	13.0

Component	Sample no.													
	71-4	99-1	99-2	99-3	99-4	99-5	100-1	100-2	100-3	100-4	100-5	100-6	100-7	100-8
SiO_2	49.55	52.14	51.77	51.94	52.88	52.37	48.37	49.98	48.43	49.42	47.6	47.11	47.64	47.89
TiO_2	0.85	0.27	0.32	0.32	0.30	0.23	0.88	1.03	0.75	0.90	1.32	1.28	0.75	0.76
Al_2O_3	6.1	2.12	1.78	2.31	1.36	1.55	7.75	7.39	7.18	9.41	8.56	9.16	7.58	6.68
FeO_{tot}	8.13	6.23	8.09	6.82	12.40	9.26	7.50	7.24	6.74	7.65	8.43	7.89	9.52	10.43
Cr_2O_3	0.26	0.35	0.13	0.41	–	0.12	0.19	0.2	0.25	0.18	0.19	–	–	0.17
MnO	0.19	0.14	0.21	0.18	0.34	0.23	0.19	0.15	0.17	0.18	0.19	0.19	0.19	0.19
NiO	–	–	–	–	–	–	–	–	–	–	–	–	0.05	0.16
MgO	15.14	17.08	18.24	17.84	18.14	19.6	13.45	14.39	13.9	12.02	13.02	12.95	12.35	12.76
CaO	20.18	20.79	18.36	19.98	15.13	16.24	22.33	21.86	22.21	20.64	22.21	22.22	21.33	20.82
Na_2O	0.12	0.22	0.28	0.26	0.15	0.24	0.34	0.28	0.31	0.7	0.36	0.93	0.43	0.07
Total	100.52	99.34	99.18	100.06	100.70	99.84	101.00	102.52	99.94	101.10	101.88	101.73	99.84	99.94
Wo	42.3	42.0	36.6	39.7	30.1	31.9	47.5	45.9	47.3	47.5	47.2	47.7	46.3	44.4
En	44.1	48.0	50.5	49.4	50.2	53.6	39.8	42	41.2	38.5	38.5	38.7	37.3	37.9
Fs	13.6	10.0	12.9	10.9	19.8	14.6	12.8	12.1	11.5	14.1	14.3	13.6	16.5	17.7

account the low concentration of MgO, these glasses were probably formed from a residual melt after fractionation of mafic minerals. A characteristic feature of these glasses is lower K_2O content as compared with the bulk host-rock analyses. Their chemical compositions (Fig. 6) are grossly similar to those of boninites from modern island arcs, for instance, the Izu–Bonin arc (Newman and van der Laan, 1992). The compositions of glasses from modern boninites are usually also much more silicic than the host lavas; and similar to the rocks studied, they tend to be depleted in potassium as compared to the bulk composition of the host rocks (Ohnenstetter and Brown, 1996a).

Thus, the rocks under investigation bear the association of magnesian mafic silicates, chromium-rich spinel, and glass of intermediate composition, which is a distinctive feature of boninite series volcanics (Crawford, 1989; Ohnenstetter and Brown, 1996b). The occurrence of rocks of this series in the Early Paleoproterozoic of the Baltic shield has been proved for the first time by petrographic and mineralogical observations. They were previously described as komatiites and komatiitic basalts on the basis of the

Table 3. Compositions of plagioclases (wt %) from the basalts of Myandukha Mountain

Component	Sample no.			
	39-1	39-2	99/1-1	99/1-2
SiO_2	52.18	53.27	51.81	52.52
Al_2O_3	30.99	30.21	31.35	31.40
FeO_{tot}	0.59	0.60	0.51	0.51
CaO	13.59	13.07	13.33	13.42
Na_2O	4.21	4.35	4.34	3.98
K_2O	0.14	0.14	0.13	0.16
Total	100.70	101.64	101.47	101.99
Or	0.8	0.8	0.7	0.9
Ab	35.6	37.3	36.8	34.6
An	63.6	61.9	62.5	64.5

occurrence of spinifex textures (Kulikov, 1988; Puchtel *et al.*, 1997, 2001), which is in conflict with the intermediate and silicic compositions of volcanic glasses. Subduction-related Phanerozoic boninitic series are dominated by the rocks of andesitic compositions. In contrast, siliceous basalts are most common among the SHMS lavas, whereas andesites and dacites occur in minor amounts. The SHMS complexes form a large intracontinental magmatic province and, correspondingly, had a different origin, which probably included extensive assimilation of the rocks of the Archean lower crust by hot mantle-derived melts.

VOLCANIC GLASS

As was noted above, volcanic glass makes up a matrix between olivine and pyroxene crystals and areas in hyaloclastites where crystallization did not occur. The glasses are spotty in back-scattered electron images, and their heterogeneous composition was revealed by microprobe analysis. The results of the instrumental investigation of the glass are presented below.

Methods of Glass Investigation

Fragments of volcanic glass, 0.3–0.5 mm in size, were mechanically recovered from crushed rocks under a binocular microscope using a needle, and this material was used to prepare suspension specimens for electron microscope examination. Glass particles and crystal phases in them were investigated on a JEM-100C transmission electron microscope equipped with an X-ray energy-dispersive spectrometer Kevex-5100, which allowed determination of the elements from Na to U. The specimen was inclined using a goniometer in order to distinguish crystalline particles among the prevailing mass of amorphous glass. Inclination produced extinction contours "running" through the crystals. This property of crystal phases allowed us to identify all phases

Table 4. Compositions of chrome spinels (wt %) from the basalts of Myandukha Mountain

Component	Sample no.									
	323-1	323-2	323-3	323-4	323-5	323-6	100-1	100-2	100-3	100-4
TiO_2	0.58	0.60	0.62	0.58	0.58	0.60	0.55	0.57	0.60	0.60
Al_2O_3	15.72	16.15	17.14	16.36	15.42	17.10	15.80	16.12	16.48	16.38
Cr_2O_3	45.16	44.53	43.5	43.96	44.71	43.96	43.77	43.74	44.31	44.49
Fe_2O_3	5.41	5.29	7.17	4.84	5.22	5.16	4.39	5.03	3.68	5.10
FeO	30.88	31.08	30.17	31.0	30.58	31.10	30.73	29.70	30.82	30.06
MnO	0.15	0.15	0.15	0.15	0.15	0.15	0.27	0.30	0.32	0.26
MgO	2.24	2.01	1.15	1.91	2.29	2.32	1.38	2.26	1.69	2.47
ZnO	0.91	1.16	1.18	1.10	0.65	0.96	1.44	1.41	1.23	1.31
Total	101.05	100.97	101.09	99.89	99.60	101.35	98.38	99.17	99.18	100.73
Al	0.63	0.64	0.66	0.66	0.62	0.68	0.65	0.65	0.67	0.65
Cr	1.21	1.19	1.13	1.19	1.21	1.16	1.21	1.19	1.21	1.19
Fe^{3+}	0.14	0.13	0.18	0.12	0.13	0.13	0.12	0.13	0.10	0.13

Note: The compositions are recalculated to four oxygen atoms.

Table 5. Compositions (wt %) of the basalts of Myandukha Mountain

Component	Sample no.														
	1	17	33	34	48	50	51	53	54	57	63	65	66	68	70
SiO_2	51.65	51.61	51.27	51.42	51.89	51.58	51.28	50.82	51.56	51.04	51.11	51.14	51.49	49.71	52.14
TiO_2	0.68	0.69	0.67	0.70	0.77	0.70	0.67	0.70	0.67	0.69	0.69	0.69	0.69	0.74	0.71
Al_2O_3	10.18	11.11	9.84	11.18	13.93	10.91	11.56	11.54	11.34	11.21	10.86	11.33	11.25	11.28	13.94
FeO_{tot}	12.21	12.04	12.32	12.40	11.10	12.53	11.99	12.28	11.93	12.29	12.26	12.22	12.39	12.59	11.5
MnO	0.18	0.19	0.18	0.19	0.17	0.18	0.18	0.19	0.18	0.19	0.19	0.19	0.19	0.20	0.17
MgO	13.72	12.50	14.58	12.02	8.31	12.34	12.32	12.14	11.91	11.98	11.8	12.08	12.22	11.76	8.15
CaO	9.44	9.61	9.17	9.69	10.15	9.46	9.42	9.70	9.82	10.21	10.75	9.74	9.28	11.61	10.79
Na_2O	1.26	1.66	1.54	1.64	2.70	1.85	1.84	1.86	1.86	1.82	1.93	1.86	1.62	1.63	1.87
K_2O	0.62	0.52	0.37	0.70	0.90	0.38	0.67	0.70	0.67	0.50	0.35	0.69	0.80	0.41	0.66
P_2O_5	0.06	0.07	0.06	0.07	0.08	0.08	0.07	0.07	0.07	0.07	0.07	0.07	0.07	0.07	0.07
Component	Sample no.														
	72	81	82	83	84	86	89	91	94	95	99	100	102	103	104
SiO_2	50.75	52.26	52.11	51.1	49.01	49.07	49.41	48.4	52.06	50.88	51.66	51.41	51.07	52.28	50.91
TiO_2	0.75	0.63	0.68	0.73	0.65	0.63	0.70	0.67	0.70	0.69	0.73	0.72	0.67	0.69	0.68
Al_2O_3	11.17	11.58	11.50	11.41	9.12	8.76	10.30	10.59	10.33	11.22	12.99	10.58	10.45	11.34	10.71
FeO_{tot}	12.75	11.45	12.34	11.88	12.38	12.41	12.38	12.47	12.09	12.07	11.88	12.44	12.67	12.39	12.68
MnO	0.18	0.17	0.19	0.19	0.19	0.19	0.20	0.20	0.19	0.19	0.18	0.19	0.19	0.19	0.19
MgO	11.03	11.25	12.17	12.47	17.81	19.09	15.52	15.96	11.85	12.43	9.99	12.99	13.49	12.13	13.38
CaO	9.99	10.31	9.39	9.70	9.32	8.80	9.54	9.81	10.39	10.13	9.94	9.33	9.23	9.25	9.13
Na_2O	2.01	1.18	1.02	1.95	1.29	0.82	1.37	1.30	1.90	1.76	1.87	1.91	1.62	1.30	1.60
K_2O	0.68	1.10	0.55	0.49	0.18	0.18	0.54	0.56	0.43	0.56	0.68	0.36	0.54	0.36	0.66
P_2O_5	0.09	0.07	0.07	0.08	0.05	0.05	0.04	0.05	0.07	0.07	0.09	0.07	0.07	0.07	0.06

Note: The analyses were obtained by the RFA method at the Institute of Geology of Ore Deposits, Petrography, Mineralogy, and Geochemistry, Russian Academy of Sciences, and are recalculated to 100%.

in the samples. A series of electron diffraction patterns and energy dispersive spectra were then obtained from the glass particles and crystal phases. The identity of mineral grains was reliably established from their structural parameters and elemental compositions.

Results

The investigation of suspension glass specimens from hyaloclastite sample no. 303 on the JEM-100C transmission electron microscope revealed ultrafine (nanometer- to micrometer-sized) crystals among numerous siliceous amorphous particles (with K admixture). Their energy-dispersive spectra displayed Si, Ca, and Fe peaks (possibly, also Al).

Numerous glass particles in electron microscope suspension specimens were represented by two morphological phases. The most common are thick structurally homogeneous silica-rich amorphous chips, often wedge-shaped with sharp edges (Fig. 9). The Si to K peak height ratio of their energy dispersive spectra is about 4 : 1. This provides semiquantitative evidence for the admixture of K in their compositions (Table 10). Among the glass particles, there are occasional lumpy aggregates of amorphous SiO_2 with a relatively loose structure. These aggregates contain a significant Ca

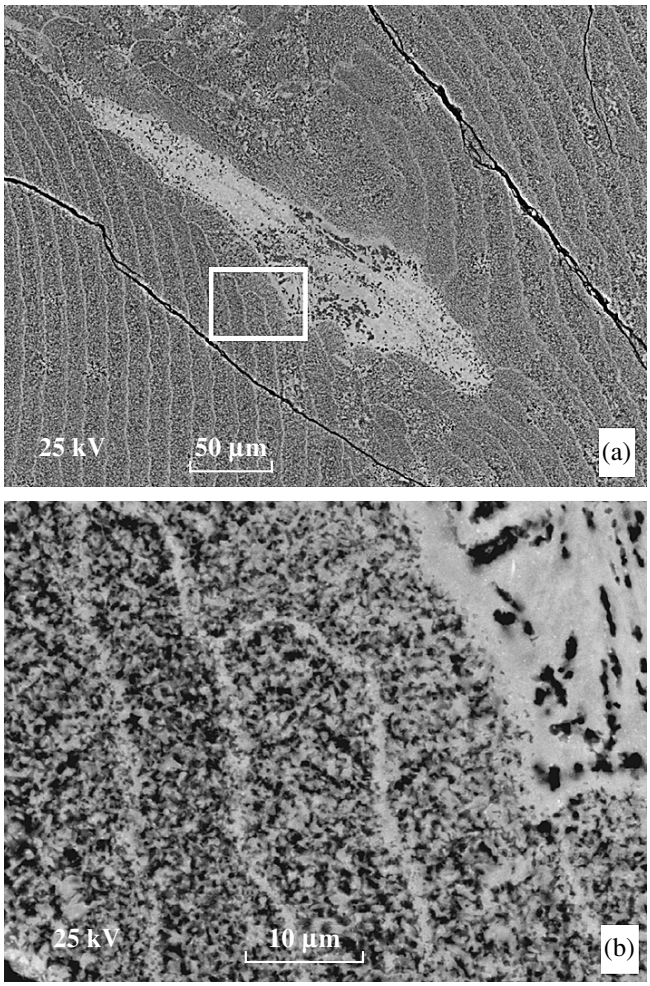

Fig. 4. Back-scattered electron images of volcanic glass with a banded fluidal structure from hyaloclastite (sample 303). (a) Overview of a crystallized area in fluidal glass. (b) Enlarged fragment.

admixture, which is indicated by a Si/Ca peak height ratio of about 4 : 1.

The second phase is represented by amorphous SiO_2 films (or plates), which contain only traces of Al, K, and Ca. The plates show a fine porous (about 10 Å) structure, which is related to the fact that they are formed by SiO_2 spheres of about the same size (Fig. 10).

In order to determine more accurately the compositions of amorphous SiO_2 particles, the suspension specimens that were prepared from hyaloclastite sample 303 for transmission electron microscopy were examined on a scanning microscope equipped with a Link ISIS spectrometer. The results are shown in Table 10. Since the back-scattered electron images obtained on the scanning microscope differ from transmission electron images, they cannot be unambiguously correlated. Therefore, the compositions presented are probably related to the both phases characterized above. The procedure of analysis on thin foils that was used by us allows only an approximate estimation of compositions (Table 10).

Both the glasslike (massive) phases and films of amorphous SiO_2 did not yield electron diffraction patterns. Only occasionally a single wide diffusive reflection of low intensity was observed, which suggested some ordering of atoms in the structure of these aggregates.

Rare crystalline minerals were found among the mass of amorphous SiO_2 particles. The analysis of electron diffraction patterns demonstrated that these crystals are mainly monoclinic and orthorhombic amphiboles (Fig. 11), whose compositions vary slightly from particle to particle (judging from variations in the heights of peaks in Kevex element spectra). In addition, some diffraction patterns suggested the presence of orthorhombic pyroxene (taking into account extinc-

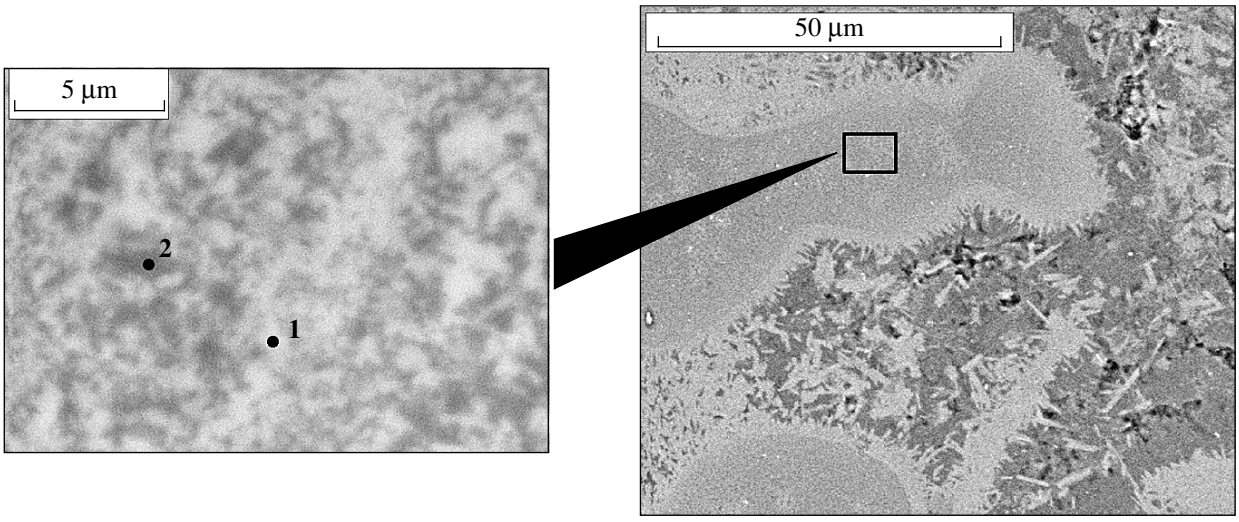

Fig. 5. Back-scattered electron image of volcanic glass with a fine spotty texture from hyaloclastite sample 303. (1) Light glass and (2) dark glass compositions are shown in Table 9.

Table 6. Compositions (wt %) of the volcanic rocks of Myandukha Mountain (traditional wet chemical analysis)

Component	Sample no.									
	301	303	304	307a	308	313	315	318	319	320
SiO_2	50.80	51.75	52.00	52.00	50.80	50.80	53.50	52.50	52.20	52.00
TiO_2	0.58	0.59	0.59	0.55	0.59	0.59	0.88	0.59	0.67	0.62
Al_2O_3	12.80	12.60	12.50	12.20	12.50	12.75	13.10	12.30	13.40	13.00
Fe_2O_3	1.64	1.50	2.73	2.51	2.74	2.73	2.13	3.11	3.31	3.34
FeO	9.30	9.32	8.32	8.54	8.20	8.25	8.56	7.56	7.82	7.48
MnO	0.17	0.18	0.18	0.17	0.17	0.18	0.17	0.18	0.18	0.19
MgO	12.15	11.20	11.27	12.07	11.33	11.95	8.16	10.59	10.21	11.12
CaO	8.60	8.48	8.18	8.48	9.17	8.02	8.54	9.24	8.10	8.38
Na_2O	1.95	2.05	2.03	1.39	1.73	1.69	2.71	1.88	2.20	1.74
K_2O	0.36	0.69	0.43	0.59	0.62	0.49	1.00	0.21	0.39	0.67
H_2O^-	<0.1	<0.1	<0.1	<0.1	<0.1	<0.1	<0.1	<0.1	<0.1	<0.1
H_2O^+	0.93	1.44	1.45	1.54	1.88	2.01	1.04	1.72	1.25	1.48
P_2O_5	0.09	0.09	0.09	0.09	0.09	0.09	0.11	0.17	0.09	0.09
CO_2	0.17	–	0.15	–	0.15	0.11	0.24	0.09	0.07	0.07
Cr_2O_3	0.09	0.14	0.10	0.11	0.13	0.17	0.10	0.10	0.10	0.14
Total	99.73	100.13	100.12	100.34	100.20	99.93	100.34	100.34	100.09	100.42

tions of reflections, the unit-cell parameters of these crystals for the same set of elements, Si, Ca, and Fe, must be about $a = 18$ and $c = 5.04$).

Epidote crystals were found occasionally. Its approximate composition based on the relative heights of element peaks is $Al_2Si_3Ca_{4.5}Fe_{1.5}$.

Another rare mineral in the samples is α-quartz. The quartz crystals were usually free of admixtures and intimately intergrown with glass, and the boundary between these phases is often rounded and sharp.

Of particular importance was the finding of an intergrowth of glass, amphibole, and several parallel pseudohexagonal microcrystals of the high-temperature SiO_2 polymorph tridymite (Fig. 12). Although tridymite is stable at 867–1470°C and low pressure, it may persist metastably upon rapid quenching or form under supergene conditions. It is remarkable that two amphibole crystals in the intergrowth have no common orientation (Fig. 12), which suggests that they crystallized from different centers under high melt oversaturation (rapid cooling).

In addition, rare grains of halite (NaCl) (Fig. 13) and the TiO_2 polymorph anatase were found. Anatase crystals were only several nanometers in size. Both these minerals occur as nanometer-sized inclusions in glass.

Micrometer-sized plates of phyllosilicates were often observed in the samples. These minerals could not be reliably identified, because we failed to obtain their space reflections along the *c* axis, which would have allowed a precise determination of unit-cell parameters. Taking into account the elemental composition of these phases, they could be represented by kaolinite (Fig. 14), chlorite, and biotite (K, Al, Si, and Fe). In a few cases, scaly particles of a phyllosilicate with the composition (Mg, Si, Fe), $a \sim 5.2$, $b \sim 9.0$, and the basal reflection d 002 ~9.2 Å (×2 = 18.4) were found. These micrometer-sized crystals are talc (Fig. 15).

In addition, aggregates of ultrafine crystals containing Al and Cu were detected. These aggregates form ring diffraction patterns corresponding to a cubic structure with $a \sim 4.28$ Å. This phase is probably an Al-bearing cuprite (Cu_2O) rather than an individual Al phase.

Thus, we demonstrated for the first time that the volcanic glass under investigation is composed of amorphous silica (with K and, occasionally, Ca admixtures) and tiny crystals (nanocrystals) of amphiboles, quartz, orthopyroxene, epidote, phyllosilicates (including talc), halite, anatase, and cuprite. All these phases are unevenly distributed in the glass providing its mottled

Table 7. Concentrations of trace elements (ppm) in the volcanic rocks of Myandukha Mountain

Element	Sample no.													
	301	302	303	304	307a	308	313	315	318	319	320	321	323	1
Sc	22	12	29	28	26	24	26	31	25	23	21	35	34	28
V	211	771	216	209	190	203	231	284	212	206	201	220	218	231
Co	62	103	62	60	48	48	60	58	54	58	46	86	78	98
Ni	204	445	187	196	191	211	186	81	173	142	167	506	240	244
Cu	110	462	93	80	93	101	62	116	81	111	88	102	106	93
Zn	107	186	91	71	75	70	95	84	91	97	74	78	83	105
Ga	–	58	–	–	–	–	–	–	–	–	–	16	17	23
Rb	18	13	18	17	25	22	18	22	9	15	23	4	12	12
Sr	161	18	189	175	157	162	188	152	169	182	165	148	197	186
Y	–	0	–	–	–	–	–	–	–	–	–	15	15	15
Zr	61	10	52	47	86	83	49	65	48	56	87	56	74	71
Nb	–	4	–	–	–	–	–	–	–	–	–	5	1	4
Ba	231	5	379	219	234	232	238	238	249	238	231	40	82	100

Element	Sample no.													
	17	33	34	48	50	51	53	54	57	63	65	66	68	70
Sc	33	45	41	44	27	39	34	25	34	28	39	39	41	29
V	221	220	235	249	236	213	218	206	218	217	218	239	232	237
Co	79	85	86	56	73	77	56	57	58	58	58	84	83	72
Ni	238	257	241	107	227	235	218	209	210	219	213	249	249	146
Cu	74	98	93	60	55	91	89	89	83	78	87	60	65	99
Zn	84	87	89	73	85	80	79	81	87	84	82	82	86	83
Ga	15	17	18	15	16	21	20	20	13	16	20	18	19	15
Rb	12	8	16	11	10	12	14	16	9	6	14	18	6	7
Sr	211	192	185	236	172	192	194	176	191	177	176	169	197	193
Y	15	14	13	20	16	17	18	18	18	17	16	15	14	14
Zr	75	76	74	78	71	71	75	75	71	74	73	76	75	72
Nb	4	9	9	6	5	5	9	8	7	8	10	6	8	5
Ba	72	77	89	109	48	109	75	89	73	56	84	91	81	77

Element	Sample no.														
	72	81	82	83	84	86	89	91	94	95	99	100	102	103	104
Sc	31	22	40	30	31	39	35	34	42	38	34	27	29	35	34
V	231	198	219	220	216	245	222	231	228	226	231	220	228	227	234
Co	61	55	55	69	66	94	86	85	69	71	69	75	83	77	86
Ni	240	201	225	231	457	504	524	482	227	234	192	220	351	231	279
Cu	280	48	94	78	95	77	101	76	38	40	95	90	78	61	86
Zn	91	82	81	83	79	89	77	86	76	83	81	80	79	87	88
Ga	14	17	22	21	21	16	11	18	15	16	17	19	17	20	24
Rb	9	13	13	11	4	15	4	11	5	11	10	8	11	9	13
Sr	193	135	213	167	137	155	137	137	141	175	195	201	201	213	180
Y	20	14	16	18	16	14	13	15	15	16	16	15	14	16	15
Zr	78	66	74	73	57	60	57	51	70	70	74	78	69	72	75
Nb	8	8	9	7	8	0	7	4	4	3	6	8	6	5	0
Ba	66	110	88	81	60	83	48	44	175	79	71	96	74	62	77

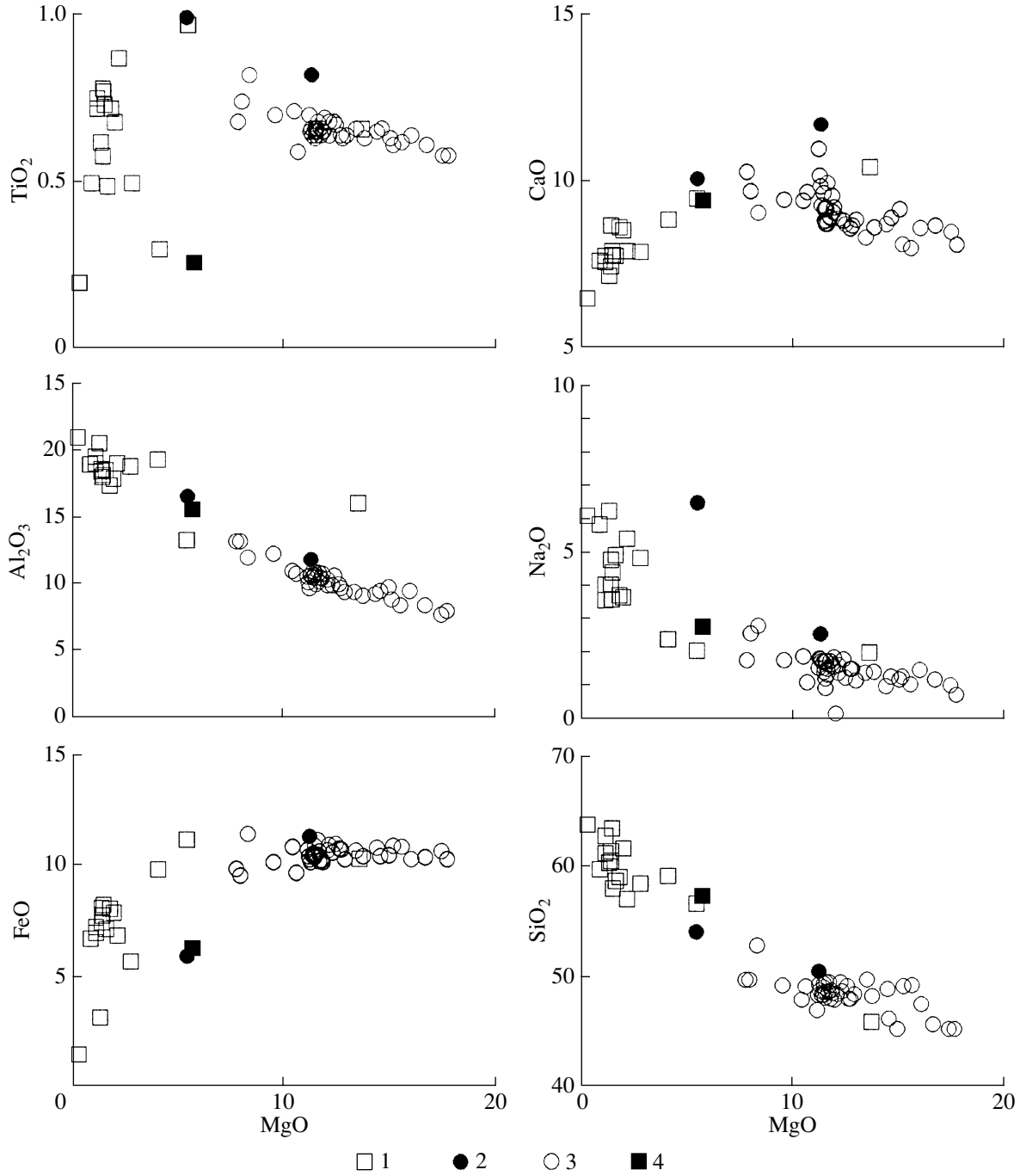

Fig. 6. Variations in the concentrations of major components (wt %) in the basalts, hyaloclastites, and volcanic glasses. (1) Glass from basalt groundmass; (2) dark and light glass from hyaloclastite sample 303; (3) basalts; (4) boninite glass from the Izu–Bonin arc (Newman and van der Laan, 1992).

appearance and variations in chemical composition between various areas.

DISCUSSION

Our study confirmed the occurrence of volcanic glass in weakly altered Early Paleoproterozoic boninite-like lavas. Several geologic and petrographic characteristics, including the occurrence as pillow lavas and hyaloclastites, microspinifex textures, skeletal forms of phenocrysts, and the presence of glass, suggest that the lavas solidified under conditions of strong supercooling in a water environment. According to our petrological results, the glasses were probably formed from residual melts between olivine and pyroxene crystals and in areas where crystallization did not occur. It

Table 8. Concentrations of REE (ppm) in the volcanic rocks of Myandukha Mountain

Element	Sample no.			
	301	304	308	315
La	9.26	8.96	8.84	10.7
Ce	19.4	19.1	18.6	22.7
Pr	2.46	2.40	2.36	3.00
Nd	10.10	9.99	9.65	11.90
Sm	2.18	2.19	2.12	2.68
Eu	0.70	0.70	0.67	0.74
Gd	2.25	2.27	2.10	2.78
Tb	0.37	0.36	0.36	0.43
Dy	2.39	2.42	2.26	2.94
Ho	0.50	0.47	0.46	0.63
Er	1.43	1.40	1.48	1.66
Tm	0.20	0.19	0.20	0.26
Yb	1.40	1.41	1.35	1.66
Lu	0.19	0.21	0.21	0.24
Total	52.83	52.07	69.66	62.32
$(La/Nd)_n$	1.76	1.72	1.75	1.72
$(Ce/Yb)_n$	3.52	3.45	3.50	3.48

Note: The analyses were obtained by the ICP-MS method at the central chemical laboratory of the Institute of Geology of Ore Deposits, Petrography, Mineralogy, and Geochemistry, Russian Academy of Sciences.

turned out that bulk-rock K_2O contents are usually higher than K_2O concentrations in the point microprobe analyses of glasses from rock groundmass (Tables 5, 6, 9). This discrepancy is probably explained by potassium concentration in discrete fine phases (e.g., biotite), which were lacking in the most clear glass areas analyzed by the microprobe.

The first detailed investigation of the second type of volcanic glass gave surprising results. It appeared that, first, the glass has a silicic composition; second, there are nanometer- and micrometer-sized crystalline phases unevenly distributed in the glass; and third, the compositions of these minerals are sharply different from those of the primary crystals of the lavas (olivine, pyroxenes, and plagioclase). Moreover, hydrous phases are predominant among such micro(nano)crystals (amphiboles, phyllosilicates, etc.). They are sometimes intergrown with tridymite, which may be a high-temperature metastable phase. This is also supported by orthopyroxene nanoinclusions. All these facts may be indicative of the primary nature of some nanoparticles not related to devitrification processes or superimposed metamorphism.

The nanoinclusions are nonuniformly distributed in the volcanic glass, which is probably responsible for its mottled texture in back-scattered electron images and considerable differences between the microprobe analyses of glasses for each particular specimen. Thus, the bulk composition of the volcanic glass is the sum of the compositions of the silica-dominated matrix and nanoinclusions. The latter are not confined to any preferential direction, which suggests that their distribution was not controlled by secondary processes and probably reflected the initial heterogeneity of the melt preserved owing to rapid quenching.

It is worth emphasizing that these nanometer- and micrometer-sized crystals are sharply different from the macroscopic crystals of the host rock, which suggests specific conditions of their formation. It is expedient

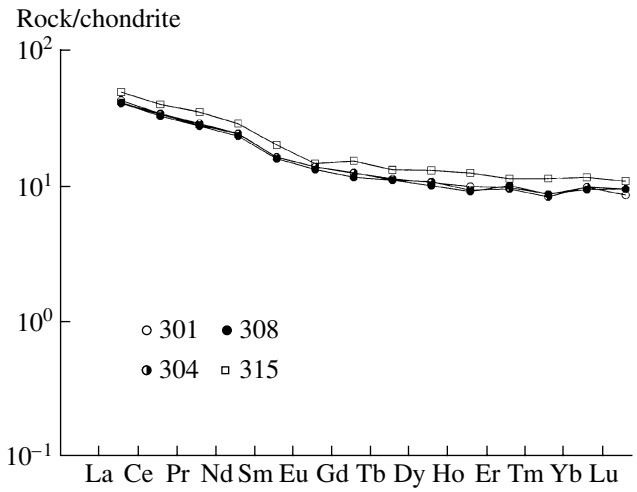

Fig. 7. Chondrite-normalized REE distribution patterns of the rocks studied. Chondrite contents are after Sun (1982).

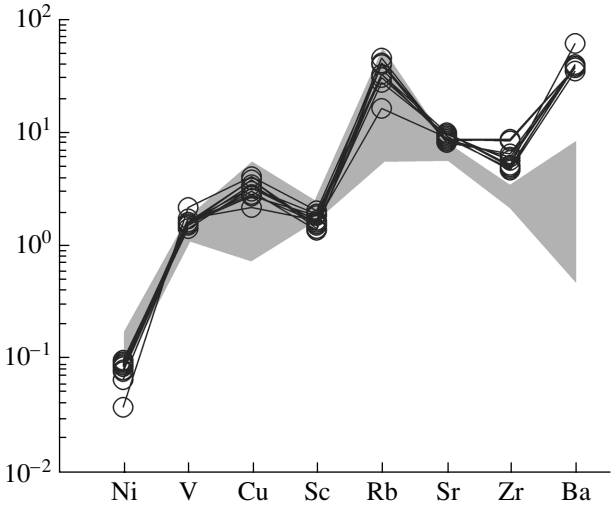

Fig. 8. Trace element distribution patterns of the basalts normalized to the primitive mantle composition (Hofmann, 1988). Also shown is the field (shaded) of boninites from the Izu–Bonin arc (Murton *et al.*, 1992).

Table 9. Compositions of volcanic glass (wt %) from the volcanic rocks of Myandukha Mountain (electron microprobe data)

Component	Sample no.											
	100-1	100-2	100-3	100-4	303-l	303-d	33-1	33-2	33-3d	33-3l	323-1	323-2
SiO_2	59.77	58.08	58.73	63.80	50.54	54.20	46.07	57.09	60.33	58.50	60.36	59.05
TiO_2	0.50	0.73	0.49	0.20	0.82	1.00	0.66	0.87	0.62	0.50	0.78	0.72
Al_2O_3	19.03	18.23	18.64	21.04	11.91	16.82	16.01	19.12	20.60	18.88	18.69	17.46
Cr_2O_3	–	0.08	–	0.04	0.18	–	–	–	–	–	–	–
FeO_{tot}	6.74	8.26	7.16	1.52	11.35	5.97	10.32	6.89	3.18	5.73	7.46	8.09
MnO	0.09	0.17	0.03	0.10	0.20	–	–	–	–	–	0.13	0.14
CaO	7.67	7.83	7.80	6.53	11.72	10.10	10.63	7.96	7.21	7.93	7.49	8.66
MgO	0.91	1.52	1.68	0.34	11.25	5.47	13.60	2.18	1.33	2.84	1.44	1.86
K_2O	0.08	0.15	0.10	0.03	0.09	–	0.18	0.10	–	–	0.66	0.35
Na_2O	5.85	4.42	4.93	6.09	2.58	6.48	1.94	5.41	6.26	4.84	4.04	3.73
P_2O_5	–	0.36	0.28	0.28	–	–	0.30	0.23	0.19	0.31	–	–
Total	100.64	99.83	99.84	99.97	100.64	100.04	99.71	99.85	99.72	99.53	101.05	100.06

Note: The letters "l" and "d" in sample numbers denote light and dark areas in mottled glasses (back-scattered electron images). Dashes denote concentrations below the microprobe detection limit.

therefore to consider our results in the context of modern concepts on glass structure. It is known that glass is an amorphous solid-state material, transitional between crystalline solid and liquid states and devoid of long-range ordering. The term glass is used for any amorphous material obtained by melt supercooling, irrespective of its chemical composition and the temperature conditions of solidification, and having the mechanical properties of solids (*Natural Glasses…*, 1987).

Among the more than 20 existing models of glass structure, the classic model by Morey (1938) agrees best with our data. According to this model, silicate glasses have amorphous differentiated structures, i.e., they cannot be regarded as perfectly homogeneous systems. They are composed of (1) a rigid silica network and (2) micelles of partially ordered silicates. The nanometer- and micrometer-sized crystals observed by us probably represent the second phase with a developed crystal structure. The micelles could crystallize

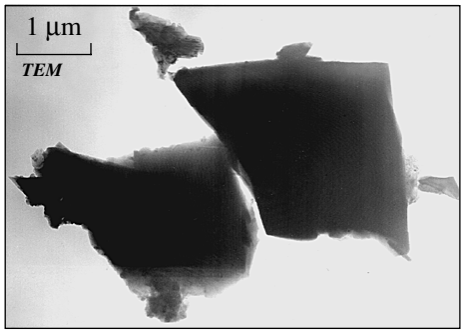

Fig. 9. Electron microprobe image of volcanic glass chips from hyaloclastite sample 303.

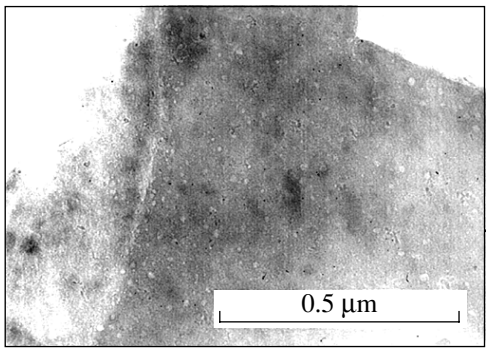

Fig. 10. Electron microscope image of the platy aggregate of tightly packed microscopic films of amorphous SiO_2 with numerous pores, about 100 Å in diameter.

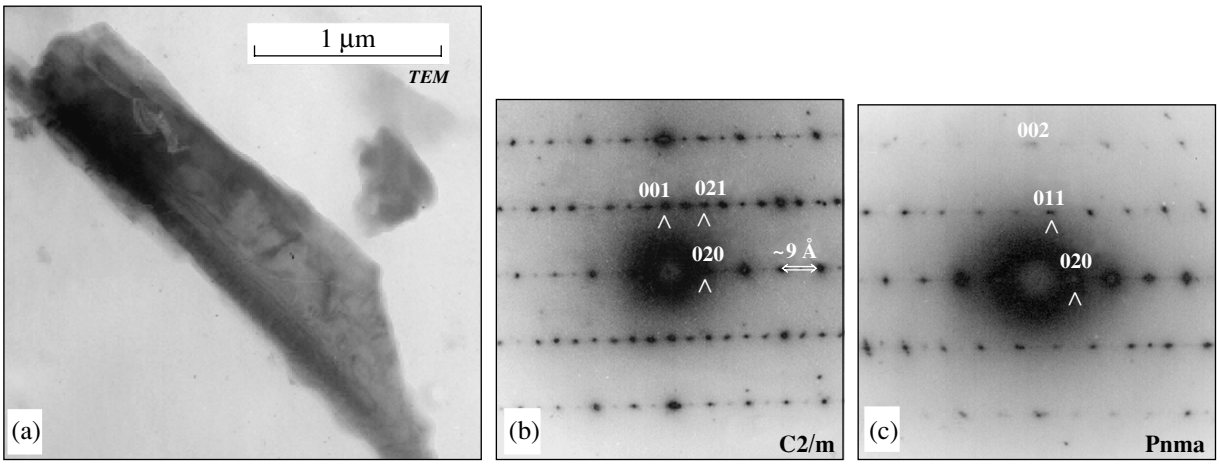

Fig. 11. (a) Intergrowth of two amphibole crystals, needle-shaped (dark zone in the lower part of the particle) and platy (lighter area in the upper part). Diffraction patterns of (b) monoclinic amphibole (tremolite) and (c) orthorhombic amphibole (anthophyllite). The corresponding space symmetry groups are shown in the lower right parts of the diffraction patterns.

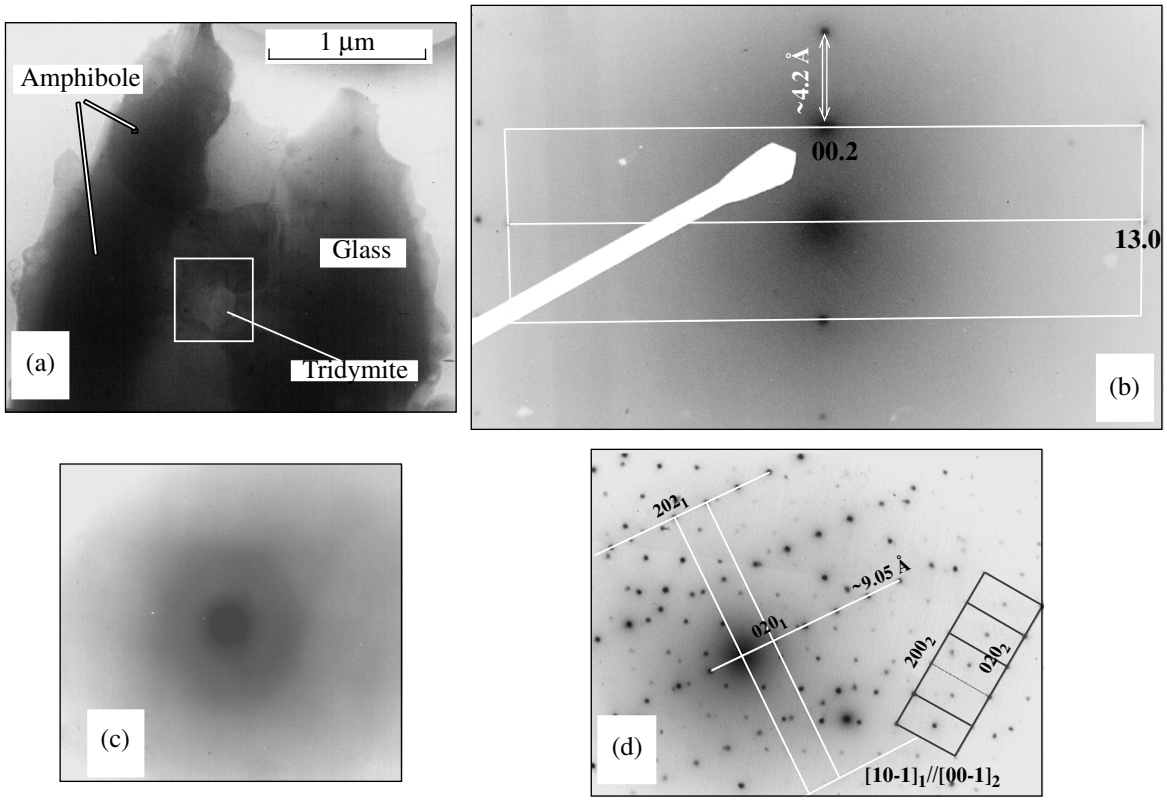

Fig. 12. (a) Electron microscope image of the intergrowth of two randomly oriented amphibole crystals, regularly aligned pseudohexagonal tridymite grains (crystals in the center), and quartz glass; (b) diffraction patterns of tridymite; (c) electronogram of quartz glass; and (d) diffraction patterns of amphibole.

either immediately after glass quenching in the hot material (orthopyroxene, tridymite, and α-quartz) or during its subsequent cooling and prolonged evolution in the Earth's crust under lower temperature conditions, when other nanocrystals were formed. Such a structure of volcanic glass (nanoinclusions of silicate minerals in silica-rich matrix) could cause its extremely long life.

CONCLUSIONS

(1) Our study confirmed the occurrence of volcanic glass in the Early Paleoproterozoic lavas of the SHMS of the Vetrenyi Poyas structure. The glass varies in composition from basalt to more common andesite and dacite and occurs in two forms: (1) uncrystallized areas of initial magmatic melt practically unaffected or very weakly affected by crystal fractionation, mainly of basic composition, and (2) residual glass in interstices between olivine and pyroxene crystals of relatively silicic, andesitic to dacitic composition. The observed association of magnesian silicates, chromium-rich spinel, and andesitic or dacitic glass allowed us to regard the volcanics as boninite-like.

(2) The glass is composed of amorphous silica with nanometer- and micrometer-sized crystals of predominant hydrous silicates (amphiboles and various phyllosilicates: chlorite, talc, biotite, and kaolinite) and occasional grains of orthopyroxene, α-quartz, tridymite, epidote, halite, anatase, and cuprite.

(3) The association of these nanometer-sized phases is fundamentally different from that of phenocrysts and lava groundmass, which includes olivine, aluminous clinopyroxene, plagioclase, and chromite. The nanometer-sized phases are unevenly distributed in the glass, which results in the mottled appearance of back-scattered electron images and variations in electron microprobe analyses. The distribution of nanocrystals was probably not controlled by any secondary process and reflected the initial heterogeneity of the melt preserved owing to rapid solidification.

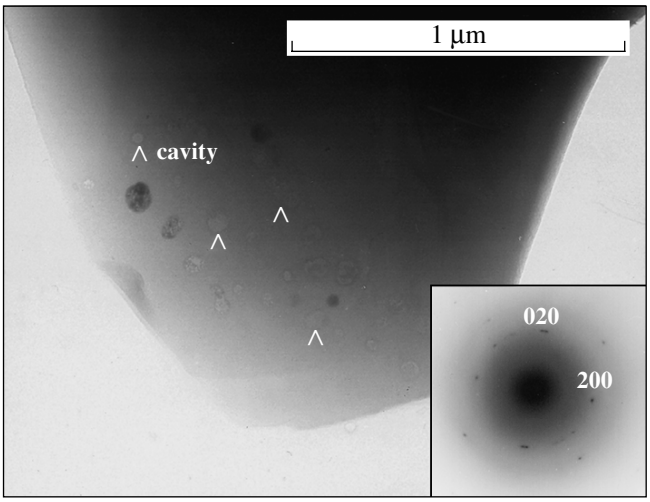

Fig. 13. Glass particles with halite microinclusions (rounded dark zones). Arrows point to numerous gas–liquid inclusions. The inset presents the electron diffraction patterns of halite.

(4) The nature of the nanophases is not yet clear. They were probably formed by the crystallization of partially ordered silicate micelles in the siliceous matrix, which occurred both immediately after glass quenching in the hot material (orthopyroxene, tridymite, and α-quartz) and during its subsequent cooling and prolonged evolution in the Earth's crust under significantly lower temperature conditions, when other nanocrystals were produced.

Table 10. Compositions of amorphous glass particles (wt %) from the hyaloclastite of Myandukha Mountain (sample 303)

Component	1	2	3	4	5	6	7	8	9	10
SiO_2	84.30	85.38	85.96	85.29	86.31	84.54	83.84	83.87	87.92	90.63
Al_2O_3	4.58	4.71	5.29	4.89	4.74	5.50	4.46	5.10	9.11	8.17
FeO_{tot}	–	–	–	0.31	–	0.83	–	–	–	–
MgO	0.53	0.31	0.93	0.37	0.53	0.99	0.63	0.72	–	–
CaO	0.26	0.39	0.97	0.24	0.45	1.37	0.31	0.47	1.92	–
Na_2O	5.81	5.28	2.95	4.23	3.99	2.28	6.17	5.21	–	–
K_2O	4.32	3.91	3.77	4.67	3.96	4.50	4.81	4.68	1.79	2.73
Total	99.80	99.98	99.87	100.00	99.98	100.01	100.22	100.05	100.74	101.53

Note: The analyses were obtained on a scanning electron microscope with an energy dispersive spectrometer.

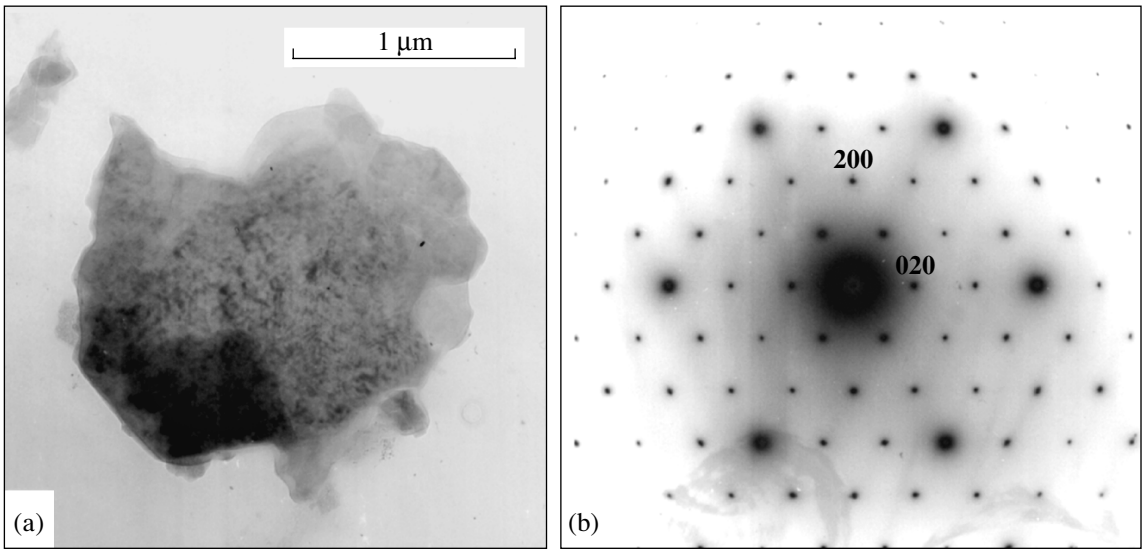

Fig. 14. (a) Platy aggregate of regularly packed scaly microscopic crystals of a clay mineral (kaolinite) and (b) single crystal point diffraction pattern of this aggregate.

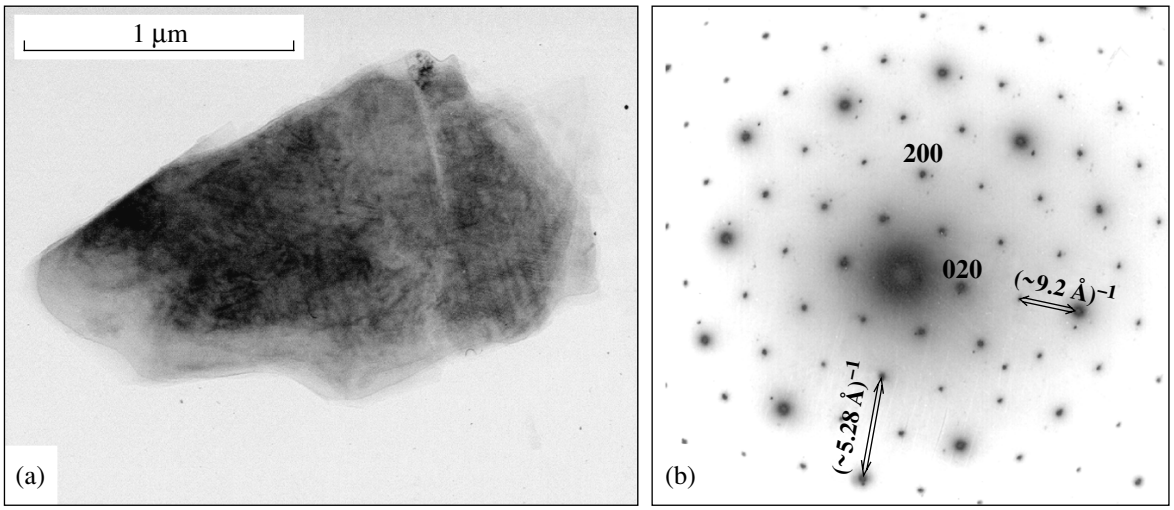

Fig. 15. (a) Intergrowth of platy talc particles and (b) its electron diffraction patterns.

ACKNOWLEDGMENTS

The authors are grateful to I.D. Ryabchikov, A.V. Girnis, A.M. Kurchavov (Institute of Geology of Ore Deposits, Petrography, Mineralogy, and Geochemistry, Russian Academy of Sciences), and O.A. Lukanin (Vernadsky Institute of Geochemistry and Analytical Chemistry, Russian Academy of Sciences) for helpful discussion of the problem. This study was financially supported by the Russian Foundation for Basic Research, project nos. 01-05-64673, 00-05-64673, and 03-05-06415, the Federal Program for the Support of Leading Scientific Schools, project no. 1251.2003.5, and Program no. 5 of the Department of Earth Sciences, Russian Academy of Sciences.

REFERENCES

1. A. D. Babansky, I. D. Ryabchikov, and O. A. Bogatikov, *Evolution of Calc-Alkaline Magmas* (Nauka, Moscow, 1983) [in Russian].
2. O. A. Bogatikov, V. I. Kovalenko, E. V. Sharkov, and V. V. Yarmolyuk, *Magmatism and Geodynamics. Terrestrial Magmatism throughout the Earth's History* (Gordon and Breach, Amsterdam, 2000).
3. A. J. Crawford, *Boninites* (Unwin Hyman, London, 1989).
4. A. V. Girnis and I. D. Ryabchikov, in *Komatiites and Highly Magnesian Volcanics of the Early Precambrian of the Baltic Shield*, Ed. by O. A. Bogatikov (Nauka, Leningrad, 1988), pp. 162–180 [in Russian].

5. A. W. Hofmann, Earth Planet. Sci. Lett. **90**, 297 (1988).
6. V. S. Kulikov, in *Komatiites and Highly Magnesian Volcanics of the Early Precambrian of the Baltic Shield*, Ed. by O. A. Bogatikov (Nauka, Leningrad, 1988), pp. 20–88 [in Russian].
7. G. W. Morey, *The Properties of Glass* (Reinhold, New York, 1938).
8. B. G. Murton, D. W. Peete, R. J. Arculus, *et al.*, Proc. Ocean Drill. Program: Sci. Results **125**, 211 (1992).
9. *Natural Glasses as Indicators of Geologic Processes*, Ed. by O. A. Bogatikov and A. M. Borsuk (Nauka, Moscow, 1987) [in Russian].
10. S. Newman and S. R. van der Laan, Proc. Ocean Drill. Program: Sci. Results **125**, 131 (1992).
11. D. Ohnenstetter and W. L. Brown, Contrib. Mineral. Petrol. **123**, 117 (1996a).
12. D. Ohnenstetter and W. L. Brown, in *Petrology and Geochemistry of Magmatic Suites of Rocks in the Continental and Oceanic Crusts*, Ed. by D. Demaiffe (ULB, Bruxelles, 1996b), pp. 307–320.
13. I. S. Puchtel, K. M. Haase, A. W. Hofmann, *et al.*, Geochim. Cosmochim. Acta **61**, 1205 (1997).
14. I. S. Puchtel, G. E. Brugmann, A. W. Hofmann, *et al.*, Contrib. Mineral. Petrol. **140**, 588 (2001).
15. E. V. Sharkov and A. S. Sindeev, Geokhimiya, No. 12, 1731 (1987).
16. E. V. Sharkov, V. F. Smolkin, and I. S. Krassivskaya, Petrologiya **5**, 503 (1997) [Petrology **5**, 448 (1997)].
17. E. V. Sharkov, O. A. Bogatikov, and I. S. Krasivskaya, Geotektonika, No. 2, 3 (2000) [Geotectonics **34**, 85 (2000)].
18. S. S. Sun, Geochim. Cosmochim. Acta **46**, 179 (1982).
19. E. B. Zolotykh, in *Petrography on the Verge of XXI Century: Results and Prospects* (Syktyvkar, 2000), Vol. 1, pp. 87–90 [in Russian].
20. E. B. Zolotykh and V. M. Ladygin, in *Paleovolcanology, Volcanosedimentary Lithogenesis, Hydrothermal Metamorphism, and Ore Formation in the Precambrian* (Petrozavodsk, 2001), pp. 143–144 [in Russian].